Sun Wei-Jie (Orcid ID: 0000-0001-5260-658X)
Slavin James, A. (Orcid ID: 0000-0002-9206-724X)
Dewey Ryan, M. (Orcid ID: 0000-0003-4437-0698)
Raines Jim, M (Orcid ID: 0000-0001-5956-9523)
Fu Suiyan (Orcid ID: 0000-0002-3858-1555)
Wei Yong (Orcid ID: 0000-0001-7183-0229)
Karlsson Tomas (Orcid ID: 0000-0002-4546-5050)
Poh Gangkai (Orcid ID: 0000-0002-5775-2006)
Jia Xianzhe (Orcid ID: 0000-0002-8685-1484)
Gershman Daniel, J (Orcid ID: 0000-0003-1304-4769)
Zong Qiu-Gang (Orcid ID: 0000-0002-6414-3794)
Wan Weixing (Orcid ID: 0000-0002-7271-5115)
Shi Quanqi (Orcid ID: 0000-0001-6835-4751)
Pu Zuyin (Orcid ID: 0000-0002-8458-6648)
Zhao Duo (Orcid ID: 0000-0001-9677-6919)

A comparative study of the proton properties of magnetospheric substorms at Earth and Mercury in the near magnetotail

W. J. Sun [1,2,3], J. A. Slavin [2], R. M. Dewey [2], J. M. Raines [2], S. Y. Fu [3], Y. Wei [1], T. Karlsson [4], G. K. Poh [2], X. Jia [2], D. J. Gershman [5], Q. G. Zong [3], W. X. Wan [1], Q Q Shi [6], Z. Y. Pu [3], D. Zhao [3]

Corresponding author: Wei-Jie Sun (wjsun@umich.edu)

[1] Key Laboratory of Earth and Planetary Physics, Institute of Geology and Geophysics, Chinese Academy of Sciences, Beijing 100029, China.

[2] Department of Climate and Space Sciences and Engineering, University of Michigan, Ann Arbor, Michigan 48109, USA.

[3] School of Earth and Space Sciences, Peking University, Beijing 100871, China.

[4] Space and Plasma Physics, School of Electrical Engineering and Computer Science, KTH Royal Institute of Technology, Stockholm, Sweden.

This is the author manuscript accepted for publication and has undergone full peer review but has not been through the copyediting, typesetting, pagination and proofreading process, which may lead to differences between this version and the Version of Record. Please cite this article as doi: 10.1029/2018GL079181

[5] Geospace Physics Laboratory, NASA Goddard Space Flight Center, Greenbelt, Maryland, USA

[6] Shandong Provincial Key Laboratory of Optical Astronomy and Solar-Terrestrial Environment, School of Space Science and Physics, Shandong University, Weihai, China

Key Points

1. Proton number densities are an order of magnitude higher, temperatures several times smaller, and κ values broader at Mercury than at Earth
2. Protons become denser and cooler during the growth phase, and are depleted and heated after the substorm dipolarizations at both planets
3. κ changes are < 20% at Earth, implying spectra-preserving accelerations, and > 60% at Mercury, implying spectra-altering accelerations

Abstract.

The variations of plasma sheet proton properties during magnetospheric substorms at Earth and Mercury are comparatively studied. This study utilizes Kappa distributions to interpret proton properties at both planets. Proton number densities are found to be around an order of magnitude higher, temperatures several times smaller, and κ values broader at Mercury than at Earth. Protons become denser and cooler during the growth phase, and are depleted and heated after the dipolarizations in both magnetospheres. The changes of κ at Earth are generally small (< 20%) indicating that

spectrum-preserving processes, like adiabatic betatron acceleration, play an important role there, while variations of κ at Mercury are large (> 60%) indicating the importance of spectrum-altering processes there, such as acceleration due to non-adiabatic cross-tail particle motions and wave-particle interactions. This comparative study reveals important intrinsic properties on the energization of protons in both magnetospheres.

Plain Language Summary

Earth and Mercury are the only two planets possessing global intrinsic magnetic fields among the four inner planets, i.e., Mercury, Venus, Earth and Mars, within the Solar System. The interactions between the intrinsic magnetic fields and the continual flow of high-speed solar wind from the Sun form similar magnetospheres at the two planets, though the scale of the magnetosphere is much smaller at Mercury than at Earth. Magnetospheric substorms, a result of solar wind–magnetosphere coupling, occur in both magnetospheres. Comparative studies of a similar process between different planets is meaningful as it can help us in understanding the specific process further as well as help us in understanding the intrinsic properties of the magnetospheres. This research paper characterizes the proton properties of magnetospheric substorms of both planets, revealing that different mechanisms control the behavior of protons during the magnetospheric substorms of the two planets.

1. Introduction

Earth and Mercury are the two planets characterized by existing global intrinsic magnetic fields among the four inner planets within the Solar System. Therefore, their magnetospheres form in the interaction between the solar wind and the global intrinsic magnetic fields and are expected to behave similarly. The Earth's magnetosphere has been extensively sampled and investigated since the 1960s (e.g., Ness, 1965), while Mercury's magnetosphere was visited only by two spacecraft, i.e., Mariner 10 (e.g., Ness, 1974) and MESSENGER (e.g., Solomon et al., 2007). Observations have revealed that Mercury's magnetosphere does share similar processes and structures with the Earth's magnetosphere (e.g., Slavin et al., 2010; Sun et al., 2015a, 2015b). Meanwhile, Mercury's magnetosphere has displayed many distinct properties (e.g., Slavin et al., 2007, 2014; Raines et al., 2015).

The magnetospheric substorm is the fundamental response in both Mercury's and Earth's magnetospheres to solar wind driving. It is a process accompanied with global magnetospheric reconfiguration, including plasma sheet thinning and thickening, plasmoid ejections and dipolarizations, and was observed to be similar at the two planets (e.g., Baker et al., 1996; Slavin et al., 2010; Sun et al., 2015a). But because the size of Mercury's magnetosphere is much smaller than the Earth's magnetosphere (e.g., Ness, 1974; Winslow et al., 2013), and the dayside magnetopause reconnection rate at Mercury is several times that at Earth (Slavin et al., 2009; DiBraccio et al., 2013), the duration of a magnetospheric substorm at Mercury (~ 2 to 3 minutes) is found to be tens of times shorter than at Earth (~ 2 to 3 hours) (e.g., Rostoker et al., 1980; Sun et al., 2015).

In the studies of plasmas sheet ion variations during the substorm at Earth, the energization and heating of ions during the dipolarizations were well observed, which were proposed to be due to the betatron and Fermi accelerations as well as processes related to induce electric fields (e.g., Williams et al., 1990; Huang et al., 1992). However, ion variations during the substorm growth phase have different results, including density and temperature increased (Williams et al., 1990); density increased but temperature constant (Nagai et al., 1997; Kistler et al., 2006); density increased but temperature decreased (Artemyev et al., 2016; Sun, Fu et al., 2017). The ion variations in the Earth's plasma sheet during the growth phase are not well understood and require further investigation.

Recently, MESSENGER observations have revealed the energization and heating of protons during Mercury's substorm dipolarizations (Sun, Raines et al., 2017; Dewey et al., 2017). Since the timescale of substorm dipolarizations (~ 5 to 10s) is comparable with the gyro-period of protons in Mercury's magnetotail, the energization of protons is expected to be non-adiabatic (e.g., Ip 1987; Delcourt et al., 2007, 2010; Sun, Raines et al., 2017). However, systematic research on the variations of proton parameters during magnetospheric substorms at Mercury remains lacking.

This study carries out a comparative study on the proton variations by employing kappa distribution to interpret the spectra during magnetospheric substorms at Mercury and Earth. Since magnetospheric substorms at the two planets not only share many similarities but also exhibit differences, it would be meaningful to comparatively study the plasma properties at the two planets during substorms. This comparative study on the proton variations reveals important intrinsic properties for the magnetospheres of both planets.

2. Observations

2.1. Instrumentations and Data Sources

This study focuses on events in the near planet tail regions, which are from –1.2 R_M to –1.8 R_M (1 R_M ~ 2440 km, a Mercury radius) at Mercury and from –7.5 R_E to –12 R_E (1 R_E ~ 6371 km, an Earth radius) at Earth. The regions of the two planets overlap considering a scaling factor of ~7–8 between the two planets (e.g., Siscoe et al., 1975). Observations at Mercury and Earth are provided by MESSENGER and THEMIS (from THD and THE) (Angelopoulos, 2008), respectively. We utilize the measurements from the Magnetometer (MAG) (Anderson et al., 2007) and the Fast Imaging Plasma Spectrometer (FIPS) (Andrews et al., 2007) onboard MESSENGER, and the Fluxgate Magnetometer (FGM) (Auster et al., 2008), the Electrostatic Analyzer (ESA) (McFadden et al., 2008) and the Solid State Telescope (SST) onboard THEMIS. The MAG provides magnetic field measurements at a time resolution of 20 vectors per second. FIPS has an energy range from ~46 eV/q to 13.3 keV/q with an effective field of view of ~1.15π sr, and a scan time of ~10 s. FIPS can distinguish different ion species through time-of-flight measurements. The FGM can provide magnetic field measurements with a time resolution of ~ 128 vectors per second, while the combined ion data from ESA and SST cover an energy range from ~5 eV to ~6 MeV over the full sky (4π sr) and at spin-resolution (3 s). However, ESA and SST cannot distinguish the different ion species.

All quantities related to the Earth's magnetosphere are presented in Geocentric Solar Magnetospheric (GSM) coordinates, where the *X* axis points toward the Sun, the *Z* axis is the projection of the Earth's magnetic dipole axis (positive North) onto the

plane perpendicular to the *X* axis, and the *Y* axis completes the right hand system. In Mercury's magnetosphere, we use the Mercury Solar Magnetospheric (MSM) coordinates, which is defined similarly to the GSM.

2.2. Case Study at Mercury

On 26 September 2011 between 12:15 and 12:19 UT, MESSENGER observed a magnetospheric substorm. In this example, MESSENGER was located in the plasma sheet, as evidenced by the number of protons with energy greater than 1 keV shown in the proton spectrum (Figure 1a). The first vertical black dashed line marks the beginning of the substorm growth phase (~ 12:16:13 UT) when B_z started to decrease notably (Figure 1d). The B_z decrease is a natural consequence of plasma sheet thinning. B_x was weak (~ 0 nT) starting at ~ 12:16:13 UT, but became more negative and deviated from the dashed red line (B_x in the preceding no substorm plasma sheet crossing) near the second vertical dashed line (Figure 1b). Meanwhile, the magnetic field elevation angle (θ) decreased (Figure 1f). Both imply the stretch of magnetic field lines. These magnetic field variations are typical features for the substorm growth phase. This substorm growth phase ended at the time marked by the second vertical dashed line (~ 12:17:50 UT), when MESSENGER detected sharp increase in B_z (Figure 1d), i.e., the dipolarization, followed by B_x decrease (Figure 1b) and B_y fluctuations (Figure 1c), which are the signatures of plasma sheet thickening and field-aligned current.

The averaged proton phase space densities (PSDs) before the substorm growth phase (Figure 1g, T1), during the substorm growth phase (Figure 1h, T2), and after the substorm dipolarization (Figure 1i, T3) are fitted with Kappa distributions. Kappa

distribution is constituted from a Maxwellian in low energy portion and a power law in high energy portion. The formula is a simple generalization of Maxwellian (e.g., Vasyliunas, 1968),

$$f_p^{\kappa}(v) = \frac{n_p}{2\pi\left(\kappa\omega_{\kappa p}^2\right)^{3/2}} \frac{\Gamma(\kappa+1)}{\Gamma(\kappa-1/2)\Gamma(3/2)} \left(1+\frac{v^2}{\kappa\omega_{\kappa p}^2}\right)^{-\kappa-1}$$

where v is the velocity of particles (proton in this study), n_p is the proton number density, Γ is the Gamma function, $\omega_{\kappa p}$ is the thermal velocity, the generalized temperature is

$$k_B T_p = \frac{\omega_{\kappa p}^2 \kappa m_p}{2\kappa - 3}$$

m_p is the proton mass and k_B is the Boltzmann constant. When $\kappa \to \infty$, this formula becomes the Maxiwellian distribution. Kappa distributions provide n_p, T_p, and κ. The index κ describes the slope of supra-thermal particle tail (>1 keV, in this study) in the distribution. In T1 (Figure 1g), the kappa distribution gives n_p ~ 2.93 ± 0.33 cm^{-3}, T_p ~ 2.34 ± 0.27 keV, and κ ~ 23.4 ± 2.67. The uncertainties were estimated in the least square curve fit on the data. In T2 (Figure 1h), the distribution gives n_p ~ 4.99 ± 0.44 cm^{-3}, T_p ~ 1.44 ± 0.13 keV, and κ ~ 3.58 ± 0.31. Protons show clear density increase by ~70%, temperature decrease by ~ –38%, and κ decrease by ~ –85% from T1 to T2. In T3 (Figure 1i), the distribution gives n_p ~ 3.61 ± 0.49 cm^{-3}, T_p ~ 3.48 ± 0.47 keV, and κ ~ 2.15 ± 0.29. Protons show number density decrease (~ –28%), temperature increase (~142%), and κ further decrease (~ –40%) from T2 to T3.

2.3. Case Study at Earth

On 24 February 2009 between ~ 06:00 UT and ~ 09:00 UT, THD observed a magnetospheric substorm at Earth in the near tail plasma sheet (~ 11 R_E). The start of the growth phase was at ~ 06:00 UT, when a clear IMF southward turning was

observed (Figure 2a, the first vertical dashed line). The second and third vertical dashed lines indicate two dipolarizations (Figures 2c to 2g) corresponding to AE increase (Figure 2b). A smooth B_z decrease was observed in the growth phase (Figure 2g, between the first and second lines), indicating a plasma sheet thinning process. Ion density (Figure 2f, n_i) and temperature (Figure 2d, T_i) derived from onboard moments show an increase from ~0.2 to ~0.55 cm^{-3} and a decrease from ~4.5 to ~2 keV, respectively. Decreases in n_i and increases in T_i were observed after the two dipolarizations.

Ion distributions in the Earth's plasma sheet usually contain more than one component, with the main component being described by a kappa distribution (e.g., Christon et al., 1991; Wing et al., 2005; Haaland et al., 2010). The main component should be mostly composed of protons (e.g., Kistler et al., 2006) in the plasma sheet. Figures 2h to 2j show three averaged ion PSDs, which are taken at the beginning of substorm growth phase (Figure 2h, T1), prior to the first dipolarization (Figure 2i, T2), and after the second dipolarization (Figure 2j, T3). We fit the main components in the three distributions with kappa distribution. In T1, the kappa fitting gives $n_i \sim 0.17 \pm 0.01$ cm^{-3}, $T_i \sim 7.84 \pm 0.52$ keV, and $\kappa \sim 9.46 \pm 0.63$. In T2, the values are $n_i \sim 0.23 \pm 0.03$ cm^{-3}, $T_i \sim 4.63 \pm 0.56$ keV, and $\kappa \sim 8.6 \pm 1.04$. From T1 to T2, ions show clear density increase (~35%) and temperature decrease (~ –41%). The κ parameter shows a small decrease (~ –9%), but the decrease is comparable with the uncertainties arising in the fitting (~6.6% for T1, ~12.1% for T2). In T3 (Figure 2j), the fitting gives $n_i \sim 0.09 \pm 0.01$ cm^{-3}, $T_i \sim 10.98 \pm 1.6$ keV, and $\kappa \sim 8.06 \pm 1.18$. Compared with the values in T2, ions show clear number density decrease (~ –61%), temperature increase (~ 137%), and a small decrease in κ (~ –6%).

The above two cases have revealed that plasma sheet protons became denser and cooler during the substorm growth phase, and were depleted and heated after the substorm dipolarizations at both planets. The κ decreases were observed during the whole substorm periods, but with the relative changes of κ at Mercury (–85% and –40%) much larger than that at Earth (–9% and –6%).

2.4. Statistical Results and Comparative Study

This section performs a statistical study focusing on the proton variations during magnetospheric substorms at both planets. At Mercury, the magnetospheric substorm cases were selected based on the criteria from Sun et al. (2015a). The cases should contain clear substorm growth and expansion phases features, i.e., MESSENGER first observed a decrease in B_z and an almost constant or increased B_x ended by a sharp increase in B_z and followed by a decrease in B_x and fluctuations in B_y. Additionally, MESSENGER was required to be located in the plasma sheet. These selection criteria give 31 satisfied cases. The proton PSDs from FIPS were averaged over ~1 min in T1, T2, and T3 for each case. In the fitting, we only select energy channels containing more than 6 counts, and at least ten channels meet this constraint, which ensures that each used energy channel contains enough counts and PSDs contain enough channels. This step is necessary since uncertainties in the plasma moments are reduced as the total counts became larger (Gershman et al., 2013). We obtain 14 qualified proton PSDs for T1, 16 for T2, and 8 for T3. At Earth, the selection criteria are similar to that of Sun, Fu, et al. (2017). The substorm growth phase started with a southward turning of IMF and ended with a substorm dipolarization in the near-Earth tail. Spacecraft should be located in the central plasma sheet during the period. We obtain 20 qualified substorm cases from THD and THE in 2008 and 2009.

The fitting results for T1, T2, and T3 at both planets are shown in Figure 3. The n_p (Figures 3a and 3b) in Mercury's plasma sheet are ~3–10 cm^{-3}, which are around an order of magnitude higher than the values in Earth's plasma sheet (~0.1–0.6 cm^{-3}). The T_p (Figures 3c and 3d) are generally several times lower at Mercury (~1–5 keV) than at Earth (~3–10 keV). The κ (Figures 3e and 3f) at Earth range mainly from ~5 to ~20, while it has a broader range of values at Mercury, which is from ~2 to ~60. The value 60 is the upper limit in our kappa fitting. At this limit the kappa distribution nearly indistinguishable from a Maxwellian distribution (e.g., Pierrard & Lazar, 2010).

In Earth's plasma sheet, n_p increases from T1 to T2 (Figure 3a) in the majority of cases (18/20), while decreases (10/20) in half and increases (10/20) in the other half from T2 to T3 (Figure 3b). In Mercury's plasma sheet, n_p typically increases from T1 to T2 (13/14, Figure 3a) and decreases from T2 to T3 (6/8, Figure 3b). The average increase ratio of n_p ($\Delta n_p/n_p$) from T1 to T2 at Mercury is 0.41 ± 0.091, which is comparable to the 0.22 ± 0.038 at Earth. At Earth, the decrease in T_p from T1 to T2 is observed in all the cases (Figure 3c), and the increase in T_p from T2 to T3 is observed in most of the cases (17/20, Figure 3d). At Mercury from T1 to T2, T_p decreases in about half of the cases (8/14) and increases in the others, while T_p increases in all the cases (8/8) from T2 to T3. The average increase ratio of T_p from T2 to T3 at Mercury is 0.36 ± 0.21, which is also comparable to the 0.14 ± 0.047 at Earth. However, changes in κ (Figures 3e and 3f) are less systematic. At Earth, κ remains similar from T1 to T2 and again from T2 to T3 (i.e., clustering around the dashed lines). At Mercury, κ often changes substantially (i.e., further away from the dashed lines) with

changes that can be positive or negative from T1 to T2 but typically negative from T2 to T3.

Figure 4 shows the histograms of $\Delta\kappa/\kappa$, where $\Delta\kappa$ are the κ changes from T1 to T2 (Figure 4a) or T2 to T3 (Figure 4b), and κ are the values in T1 (Figure 4a) or T2 (Figure 4b). In Figure 4a, blue bars (Earth cases) are distributed near ~0 with a mean value of 0.07 ± 0.071, while the red bars (Mercury cases) distribute mostly away from ~0, with the mean value of only negative bars of –0.67 ± 0.102. In Figure 4b, blue and red bars distribute in a similar way to Figure 4a with the mean values of blue bars being –0.04 ± 0.048 and red bars –0.61 ± 0.054. These statistical results on κ changes confirm the results in our case studies. The relative changes of κ of protons during the substorm at Mercury are larger than that at Earth.

3. Conclusion and Discussion

The variations of protons during magnetospheric substorms at Earth and Mercury are comparatively studied with the measurements from MESSENGER and THEMIS. This study utilizes Kappa distributions to interpret plasma sheet protons properties. It is found that n_p is about an order of magnitude higher in Mercury's plasma sheet (~3–10 cm^{-3}) than in Earth's (~0.1–0.6 cm^{-3}). The T_p is generally several times lower at Mercury (~1–5 keV) than at Earth (~3–10 keV). The κ at Earth mainly concentrates from ~5 to ~20, while it has a broader range of values (from ~2 to ~60) at Mercury. In most cases, plasma sheet protons become denser and cooler during the substorm growth phase and are depleted and heated after the substorm dipolarizations at both planets. The changes of κ during the substorms at Earth are small (<20%), but are much larger at Mercury (>60%).

The small variations of κ during the magnetospheric substorm in Earth's plasma sheet indicate that spectrum-preserving processes, like betatron acceleration under the conservation of magnetic moment ($\Delta W_{\perp} = W_{\perp}\Delta B/B$, where W is the particle energy, and B is the strength of magnetic field), play an important role. Charged particles at all energies would maintain relatively the same proportional energy and would not change the shape of high-energy tail under betatron acceleration (e.g., Christon et al., 1991). During the growth phase, B_z in the magnetic equatorial plane would decrease as a natural consequence of plasma sheet thinning, which suggested that protons would experience adiabatic betatron cooling and, therefore, result in T_p decrease. During the substorm dipolarization, the sharp B_z increase would cause strong betatron heating (T_p increase) for the protons.

At Mercury, the large variations of κ during the magnetospheric substorm indicate the importance of spectrum-altering processes, i.e., energy-dependent energy increments. We propose two possible candidates for the spectrum-altering processes. One is the acceleration due to non-adiabatic cross-tail particle motion associated with thin current sheets (e.g., Speiser, 1965; Lyons & Speiser, 1982; Ashour-Abdalla et al., 1990). In Mercury's magnetotail, the field line radius of curvature in the equatorial plane is ~200 km on average (Rong et al., 2018). The 0.1 keV protons gyrating in a magnetic field of 10 nT would have a gyroradius of ~160 km comparable to the average radius of curvature. On the other hand, the 1 keV protons could have a gyroradius of ~ 500 km comparable to the mean thickness of Mercury's tail current sheet (~ 800 km) (Poh et al., 2017a). Thus, protons would predominately move in the way of non-adiabatic cross-tail particle motion in Mercury's magnetotail. Lyons & Speiser (1982) showed that this cross-tail acceleration is sensitive to the ratio of the

dawn-to-dusk electric field (E_y) to the vertical B_z. The high E_y due to relatively high cross-tail potential (Slavin et al., 2009, 2010; DiBraccio et al., 2015; Jasinski et al., 2017) would result in strong cross-tail acceleration for protons at Mercury. The other possible candidate is wave-particle interactions (e.g., Hasegawa et al., 1985; Shizgal, 2007; Catapano et al., 2017). For the case in Figure 1, we do observe intense plasma waves with frequencies around the proton gyrofrequency, especially after the dipolarization in the wavelet spectrum of MAG data (see supporting information). This could be electromagnetic ion cyclotron (EMIC) waves, which were often observed in the Mercury's plasma sheet (Schriver et al., 2011). The accumulated pitch angle-energy distribution for protons show loss cone feature suggesting possible mechanism for EMIC (see supporting information). Therefore, wave-particle interactions might also contribute to the changes of κ during the substorm at Mercury. It needs to note that this paragraph discuss two straightforward possibilities for the spectrum altering processes at Mercury. Other mechanisms could still play a role in the process.

There are several cases at Earth showing $|\Delta\kappa/\kappa| > 0.4$ (Figure 4), indicating that spectrum-altering processes also exist in Earth's plasma sheet during magnetospheric substorms as proposed by previous studies (e.g., Christon et al., 1991; Huang et al., 1992). The magnetospheric substorm case at Earth shown in Figure 2 did contain plasma waves with frequency around the proton gyrofrequency (see supporting information). Since most of the cases at Mercury show $|\Delta\kappa/\kappa| > 0.4$, the spectrum-altering processes during the magnetospheric substorm at Earth might not be as intense as that at Mercury. This reveals that, during the magnetospheric substorms, protons could be well described by adiabatic betatron acceleration at Earth, while spectrum-altering acceleration processes dominate the behavior of protons at

Mercury. We suggest this different character of protons could closely relate to the distinct properties of the two magnetospheres. Most importantly, the scale of Mercury's magnetosphere is much smaller than that of Earth's magnetosphere (e.g., Siscoe et al., 1975; Winslow et al., 2013). The relatively thin plasma sheet and small radius of curvature of the magnetic field lines in Mercury's magnetotail (e.g., Poh et al., 2017a, 2017b; Rong et al., 2018) would make spectrum altering processes important.

Acknowledgement.

MESSENGER data used in this study were available from the Planetary Data System (PDS): http://pds.jpl.nasa.gov. The MESSENGER project is supported by the NASA Discovery Program under contracts NASW-00002 to the Carnegie Institution of Washington and NAS5-97271 to The Johns Hopkins University Applied Physics Laboratory. We acknowledge NASA contract NAS5-02099 and V. Angelopoulos for use of data from the THEMIS Mission (available at http://themis.ssl.berkeley.edu/.). Specifically: D. Larson and R. P. Lin for use of SST data, C. W. Carlson and J. P. McFadden for use of ESA data, K. H. Glassmeier, U. Auster and W. Baumjohann for the use of FGM data provided under the lead of the Technical University of Braunschweig and with financial support through the German Ministry for Economy and Technology and the German Center for Aviation and Space (DLR) under contract 50 OC 0302. We also acknowledge use of NASA/GSFC's Space Physics Data Facility's OMNIWeb service (OMNI data is downloaded from http://omniweb.gsfc.nasa.gov/) and World Data Center for Geomagnetism, Kyoto (AE, AL data, http://wdc.kugi.kyoto-u.ac.jp/). WJS is funded by National Postdoctoral Program for Innovative Talents (grant BX201600158) and China Postdoctoral Science Foundation (grant 2016M600124). This work is supported by the National Nature Science Foundation of China (grants 41704163, 41525016, 41474155, 41474139, 41661164034). YW is supported by Thousand Young Talents Program of China. The contributions by one of the authors (JAS) were supported by NASA's Heliophysics Supporting Research (NNX15AJ68G) and Living With a Star (NNX16AJ67G) programs. JMR and DJG were suppored by NASA's Discovery Data Analysis Program (NNX16AJ05G). This work is also supported by the CAS Key Laboratory of Lunar and Deep Space Exploration through grant 2013DP173157. Wei-Jie Sun thanks Dr. Xuzhi Zhou (School of Earth and Space Sciences, Peking University) for helpful

discussions.

References

Anderson, B. J., Acuña, M. H., Lohr, D. A., Scheifele, J., Raval, A., Korth, H., & Slavin, J. A. (2007). The magnetometer instrument on MESSENGER. *Space Science Reviews*, 131, 417. https://doi.org/10.1007/s11214-007-9246-7

Anderson, B. J., Johnson, C. L., Korth, H., Purucker, M. E., Winslow, R. M., Slavin, J. A., … Zurbuchen, T. H. (2011). The global magnetic field of Mercury from MESSENGER orbital observations. *Science*, 333, 1859–1862. https://doi.org/10.1126/science.1211001

Andrews, G., Zurbuchen, T. H., Mauk, B. H., Malcom, H., Fisk, L. A., Gloeckler, G., … Raines, J. M. (2007). The energetic particle and plasma spectrometer instrument on the MESSENGER spacecraft. *Space Science Reviews*, 131, 523. https://doi.org/10.1007/s11214-007-9272-5

Angelopoulos, V. (2008). The THEMIS Mission. *Space Science Reviews*, 141(1-4), 5–34. https://doi.org/10.1007/s11214-008-9336-1

Artemyev, A. V., Angelopoulos, V., Runov, A., & Petrokovich, A. A. (2016). Properties of current sheet thinning at x ~ -10 to -12 RE. *Journal of Geophysical Research: Space Physics*, 121, 6718–6731. https://doi.org/10.1002/2016JA022779

Ashour-Abdalla, M., Berchem, J., Büchner, J., & Zelenyi, M. (1990) Chaotic scattering and acceleration of ions in the Earth's magnetotail, *Geophysical Research Letters*, 17, 2317.

Auster, H. U., Glassmeier, K. H., Magnes, W., Aydogar, O., Baumjohann, W., Constantinescu, D., … Wiedemann, M. (2008). The THEMIS fluxgate magnetometer. *Space Science Reviews*, 141(1–4), 235–264. https://doi.org/10.1007/s11214-008-9365-9

Baker, D. N., Dewey, R. M., Lawrence, D. J., Goldsten, J. O., Peplowski, P. N., Korth, H., … Solomon, S. C. (2016). Intense energetic electron flux enhancements in Mercury's magnetosphere: An integrated view with high-resolution observations from MESSENGER. *Journal of Geophysical Research: Space Physics*, 121, 2171–2184. https://doi.org/10.1002/2015JA021778

Baker, D. N., Pulkkinen, T. I., Angelopoulos, V., Baumjohann, W., & McPherron, R. L. (1996). Neutral line model of substorms: Past results and present view. *Journal of Geophysical Research*, 101(A6), 12,975–13,010. https://doi.org/10.1029/95JA03753

Catapano, F., Zimbardo, G., Perri, S., Greco, A., Delcourt, D., Retino, A., & Cohen, I. J. (2017). Charge proportional and weakly mass-dependent acceleration of different ion species in the Earth's magnetotail. *Geophysical Research Letters*, 44, 10,108–10,115.

https://doi.org/10.1002/2017GL075092

Christon, S. P., Williams, D. J., Mitchell, D. G., Huang, C. Y., & Frank, L. A. (1991), Spectral characteristics of plasma sheet ion and electron populations during disturbed geomagnetic conditions, *Journal of Geophysical Research: Space Physics*, 96(A1), 1-22.

Delcourt, D. C., Leblanc, F., Seki, K., Terada, N., Moore, T. E., & Fok, M. C. (2007), Ion energization during substorms at Mercury, *Planetary and Space Science*, 55(11), 1502–1508

Delcourt, D. C., Moore, T. E., & Fok, M.-C. H. (2010). Ion dynamics during compression of Mercury's magnetosphere. *Annales de Geophysique*, 28, 1467–1474. https://doi.org/10.5194/angeo-28-1467-2010

Delcourt, D. C., Seki, K., Terada, N., & Miyoshi, Y. (2005), Electron dynamics during substorm dipolarization in Mercury's magnetosphere, *Annales de Geophysique*, 23(10), 3389-3398.

Dewey, R. M., Slavin, J. A., Raines, J. M., Baker, D. N., & Lawrence, D. J. (2017). Energetic electron acceleration and injection during dipolarization events in Mercury's magnetotail. *Journal of Geophysical Research: Space Physics*, 122, 12,170–12,188. https://doi.org/10.1002/2017JA024617

DiBraccio, G. A., Slavin, J. A., Boardsen, S. A., Anderson, B. J., Korth, H., Zurbuchen, T. H., … Solomon, S. C. (2013). MESSENGER observations of magnetopause structure and dynamics at Mercury. *Journal of Geophysical Research: Space Physics*, 118, 997–1008. https://doi.org/10.1002/jgra.50123

DiBraccio, G. A., Slavin, J. A., Raines, J. M., Gershman, D. J., Tracy, P. J., Boardsen, S. A.,…Solomon, S. C. (2015). First observations of Mercury’s plasma mantle by MESSENGER. *Geophysical Research Letters*, 42, 9666–9675. https://doi.org/10.1002/2015GL065805

Gershman, D. J., Slavin, J. A., Raines, J. M., Zurbuchen, T. H., Anderson, B. J., Korth, H., Baker, D. N., & Solomon S. C. (2013), Magnetic flux pileup and plasma depletion in Mercury's subsolar magnetosheath, *Journal of Geophysical Research: Space Physics*, 118, 7181–7199, https://doi.org/10.1002/2013JA019244.

Gershman, D. J., Slavin, J. A., Raines, J. M., Zurbuchen, T. H., Anderson, B. J., Korth, H., Baker, D. N., & Solomon S. C. (2014), Ion kinetic properties in Mercury's pre−midnight plasma sheet, *Geophysical Research Letters*, 41, 5740–5747, https://doi.org/10.1002/2014GL060468.

Haaland, S., Kronberg, E. A., Daly, P. W., Fränz, M., Degener, L., Georgescu, E., & Dandouras, I. (2010), Spectral characteristics of protons in the Earth's plasmasheet: statistical results from Cluster CIS and RAPID, *Annales de Geophysique*, 28(8), 1483-1498.

Hasegawa, A., K. Mima, and M. Duong‐van (1985), Plasma distribution function in a superthermal radiation field, *Phys. Rev. Lett.*, **54**, 2608–2610, doi:10.1103/PhysRevLett.54.2608.

Hones Jr., E. W. (1977), Substorm processes in the magnetotail: Comments on 'On hot tenuous plasmas, fireballs, and boundary layers in the Earth's magnetotail' by L. A. Frank, K. L. Ackerson, and R. P. Lepping, *Journal of Geophysical Research*, 82(35), 5633–5640, doi:10.1029/JA082i035p05633.

Huang, C. Y., Frank, L. A., Rostoker, G., Fennell, J., & Mitchell D. G. (1992), Nonadiabatic heating of the central plasma sheet at substorm onset, *Journal of Geophysical Research*, 97(A2), 1481–1495, doi:10.1029/91JA02517.

Imber, S. M., & Slavin, J. A. (2017). MESSENGER observations of magnetotail loading and unloading: Implications for substorms at Mercury. *Journal of Geophysical Research: Space Physics*, 122. https://doi.org/10.1002/2017JA024332

Ip, W. H. (1987), Dynamics of electrons and heavy ions in Mercury's magnetosphere, *Icarus*, 71(3), 441-447.

Jasinski, J. M., Slavin, J. A., Raines, J. M., & DiBraccio, G. A. (2017). Mercury's solar wind interaction as characterized by magnetospheric plasma mantle observations with MESSENGER. *Journal of Geophysical Research: Space Physics*, 122. https://doi.org/10.1002/2017JA024594

Kistler, L. M., Mouikis, C. G., Cao, X., Frey, H., Klecker, B., Dandouras, I., … Lucek, E. (2006). Ion composition and pressure changes in storm time and nonstorm substorms in the vicinity of the near-earth neutral line. *Journal of Geophysical Research*, 111, A11222. https://doi.org/ 10.1029/2006JA011939

Lyons, L. R., & Speiser, T. W. (1982). Evidence for current sheet acceleration in the geomagnetic tail, *Journal of Geophysical Research*, 87(A4), 2276–2286, doi:10.1029/JA087iA04p02276.

McFadden, J. P., Carlson, C. W., Larson, D., Ludlam, M., Abiad, R., Elliott, B., … Angelopoulos, V. (2008). The THEMIS ESA plasma instrument and in-flight calibration. *Space Science Reviews*, 141(1-4), 277–302. https://doi.org/10.1007/s11214-008-9440-2

Nagai, T., Mukai, T., Yamamoto, T., Nishida, A., Kokubun, S., & Lepping, R. P. (1997). Plasma sheet pressure changes during the substorm growth phase. *Geophysical Research Letters*, 24(8), 963–966. https://doi.org/10.1029/97GL00374

Ness, N. F. (1965), The Earth's magnetic tail, *Journal of Geophysical Research*, 70(13), 2989–3005, doi:10.1029/JZ070i013p02989.

Ness, N. F., Behannon, K. W., Lepping, R. P., Whang, Y. C., & Schatten, K. H. (1974). Magnetic field observations near Mercury: Preliminary results from mariner 10. *Science*, 185(4146), 151–160. https://doi.org/10.1126/science.185.4146.151

Pierrard, V., & Lazar, M., (2010). Kappa distributions: Theory and applications in space plasmas, *Solar Physics*, 267(1), 153–174.

Poh, G., Slavin, J. A., Jia, X., Raines, J. M., Imber, S. M., Sun, W. J., … Smith, A. W. (2017a). Mercury's cross-tail current sheet: Structure, X-line location and stress balance. *Geophysical Research Letters*, 44, 678–686. https://doi.org/10.1002/2016GL071612

Poh, G., Slavin, J. A., Jia, X., Raines, J. M., Imber, S. M., Sun, W. J., … Smith, A. W. (2017b). Coupling between Mercury and its nightside magnetosphere: Cross‐tail current sheet asymmetry and substorm current wedge formation, *Journal of Geophysical Research: Space Physics*, 122, 8419–8433. https://doi.org/10.1002/2017JA024266

Raines, J. M., DiBraccio, G. A., Cassidy, T. A., Delcourt, D. C., Fujimoto, M., Jia, X.,…Wurz, P. (2015). Plasma sources in planetary magnetospheres: Mercury. *Space Science Reviews*, 192(1–4), 91–144. https://doi.org/10.1007/s11214-015-0193-4

Rong, Z. J., Ding, Y., Slavin, J. A., Zhong, J., Poh, G., Sun, W. J., … Shen, C. (2018). The magnetic field structure of Mercury's magnetotail. *Journal of Geophysical Research: Space Physics*, 123, 548–566. https://doi.org/10.1002/2017JA024923

Rostoker, G., Akasofu, S.-I., Foster, J., Greenwald, R., Kamide, Y., Kawasaki, K., Lui, A., McPherron, R., & Russell C. (1980). Magnetospheric substorms—definition and signatures, *Journal of Geophysical Research*, 85(A4), 1663–1668, doi:10.1029/JA085iA04p01663.

Schriver, D., Trávníček, P. M., Anderson, B. J., Ashour-Abdalla, M., Baker, D. N., Benna, M., … , Zurbuchen, T. H. (2011), Quasi-trapped ion and electron populations at Mercury, *Geophysical Research Letters*, 38, L23103, doi:10.1029/2011GL049629.

Shizgal, B. D. (2007). Suprathermal particle distributions in space physics: Kappa distributions and entropy, *Astrophysics and Space Science*, 312(3), 227–237. https://doi.org/10.1007/s10509-007-9679-1

Simpson, J. A., Eraker, J. H., Lamport, J. E., & Walpole, P. H. (1974). Electrons and protons accelerated in Mercury's magnetic field. *Science*, 185, 160–166.

Siscoe, G. L., Ness, N. F., & Yeates, C. M. (1975), Substorms on Mercury? *Journal of Geophysical Research*, 80(31), 4359-4363. https://doi.org/10.1029/JA080i031p04359

Slavin, J. A., Acuña, M. H., Anderson, B. J., Baker, D. N., Benna, M., Board, S. A., … Zurbuchen, T. H. (2009). MESSENGER observations of magnetic reconnection in Mercury's magnetosphere. *Science*, 324, 606–610. https://doi.org/10.1126/science.1172011

Slavin, J. A., Anderson, B. J., Baker, D. N., Benna, M., Boardsen, S. A., Gloeckler, G., … Zurbuchen, T. H. (2010). MESSENGER observations of extreme loading and unloading of Mercury's magnetic tail. *Science*, 329(5992), 665–668. https://doi.org/10.1126/science.1188067

Slavin, J. A., Krimigis, S. M., Acuña, M. H., Anderson, B. J., Baker, D. N., Koehn, P. L., …Zurbuchen, T. H. (2007). MESSENGER: Exploring Mercury's magnetosphere. *Space Science Reviews*, 131(1–4), 133–160. https://doi.org/10.1007/s1/214-007-9154-x

Slavin, J. A., DiBraccio, G. A., Gershman, D. J., Imber, S. M., Poh, G. K., Raines, J. M., … Solomon, S. C. (2014). MESSENGER observations of Mercury's dayside magnetosphere under extreme solar wind conditions. Journal of Geophysical Research: Space Physics, 119, 8087–8116. https://doi.org/10.1002/2014JA020319

Solomon, S., McNutt Jr, R. L., Gold, R. E., & Domingue, D. L. (2007). MESSENGER mission overview. *Space Science Reviews*, 131, 3–39. https://doi.org/10.1007/%20s11214-007-9247-6

Speiser, T. W. (1965). Particle trajectories in model current sheets: 1. Analytical solutions, *Journal of Geophysical Research*, 70(17), 4219–4226, doi:10.1029/JZ070i017p04219.

Sun, W. J., Fu, S. Y., Slavin, J. A., Raines, J. M., Zong, Q. G., Poh, G. K., & Zurbuchen, T. H. (2016). Spatial distribution of Mercury's flux ropes and reconnection fronts: MESSENGER observations. *Journal of Geophysical Research: Space Physics*, 121, 7590–7607. https://doi.org/10.1002/2016JA022787

Sun, W. J., Fu, S. Y., Wei, Y., Yao, Z. H., Rong, Z. J., Zhou, X. Z., … Shen, X. C. (2017). Plasma

sheet pressure variations in the near-Earth magnetotail during substorm growth phase: THEMIS observations. *Journal of Geophysical Research: Space Physics*, 122, 12,212–12,228. https://doi.org/10.1002/2017JA024603

Sun, W. J., Raines, J. M., Fu, S. Y., Slavin, J. A., Wei, Y., Poh, G. K., …Wan, W. X. (2017). MESSENGER observations of the energization and heating of protons in the near-Mercury magnetotail. *Geophysical Research Letters*, 44, 8149–8158. https://doi.org/10.1002/2017GL074276

Sun, W.-J., Slavin, J. A., Fu, S., Raines, J. M., Sundberg, T., Zong, Q.-G., … Zurbuchen, T. H. (2015), MESSENGER observations of Alfvénic and compressional waves during Mercury's substorms, *Geophysical Research Letters*, 42, 6189–6198, doi://doi.org/10.1002/2015GL065452.

Sun, W.-J., Slavin, J. A., Fu, S., Raines, J. M., Zong, Q. G., Imber, S. M., … Baker, D. N. (2015). MESSENGER observations of magnetospheric substorm activity in Mercury's near magnetotail. *Geophysical Research Letters*, 42, 3692–3699. https://doi.org/10.1002/2015GL064052

Vasyliunas, V. M. (1968), A survey of low-energy electrons in the evening sector of the magnetosphere with OGO 1 and OGO 3, *Journal of Geophysical Research*, 73(9), 2839–2884, doi:10.1029/JA073i009p02839.

Williams, D. J., Mitchell, D. G., Huang, C. Y., Frank, L. A., & Russell, C. T. (1990). Particle acceleration during substorm growth and onset, *Geophysical Research Letters*, 17(5), 587–590, doi:10.1029/GL017i005p00587.

Wing, S., Johnson, J. R., Newell, P. T., & Meng, C.-I. (2005), Dawn-dusk asymmetries, ion spectra, and sources in the northward interplanetary magnetic field plasma sheet, *Journal of Geophysical Research*, 110, A08205, doi:10.1029/2005JA011086.

Winslow, R. M., Anderson, B. J., Johnson, C. L., Slavin, J. A., Korth, H., Purucker, M. E., … Solomon, S. C. (2013). Mercury's magnetopause and bow shock from MESSENGER Magnetometer observations. *Journal of Geophysical Research: Space Physics*, 118, 2213–2227. https://doi.org/10.1002/jgra.50237

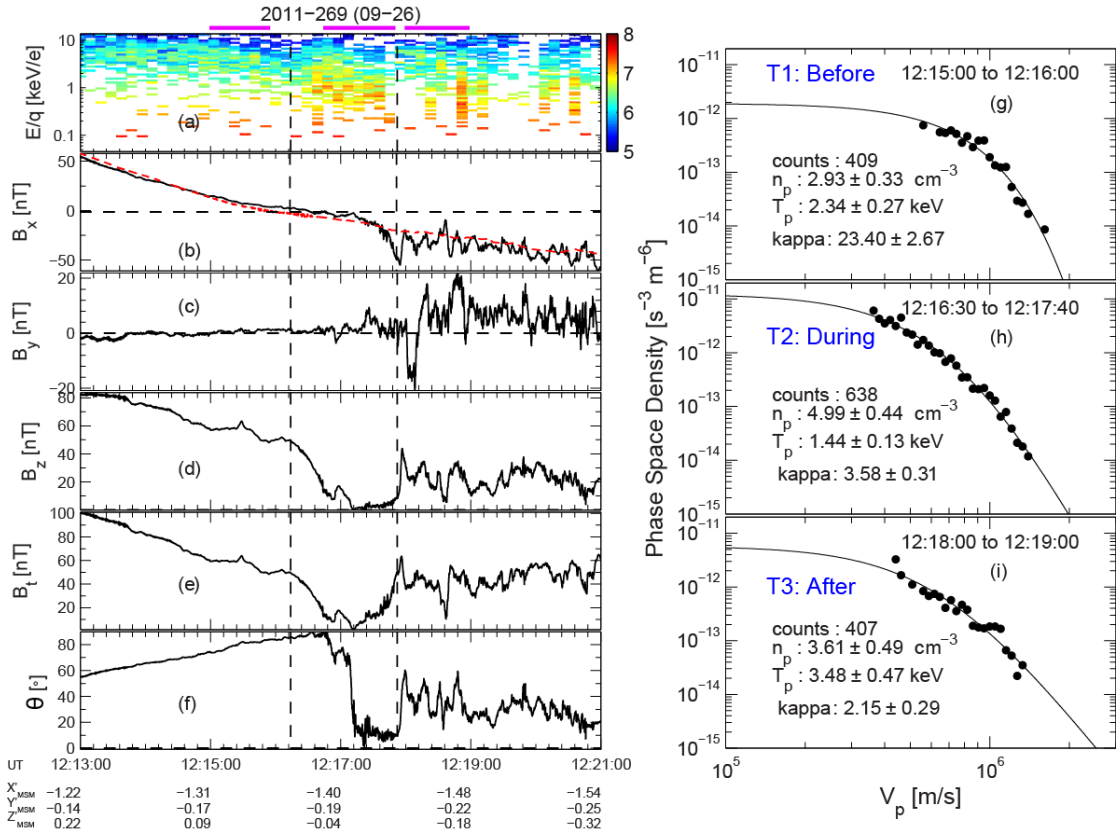

Figure 1. MESSENGER observations of a magnetospheric substorm at Mercury. (a) Energy spectrum for protons, in $\log_{10}$ (keV sr s cm^2)$^{-1}$; (b) magnetic field X component, B_x. dashed red line represents the B_x of the preceding plasma sheet crossing with no substorm signature. (c) B_y; (d) B_z; (e) B_t; (f) magnetic elevation angle, θ = atan(B_z/B_x); (g) averaged proton phase space density (PSD) from 12:15:00 to 12:16:00, prior to the substorm growth phase (T1 : Before); (h) averaged proton PSD from 12:16:30 to 12:17:40, during the substorm growth phase (T2 : During); and (i) averaged proton PSD from 12:18:00 to 12:19:00, after the substorm dipolarization (T3 : After). Black lines in Figures 1g to 1i are the kappa fitting results for the PSDs. The magenta marks above panel (a) indicate the durations for T1, T2, and T3, respectively.

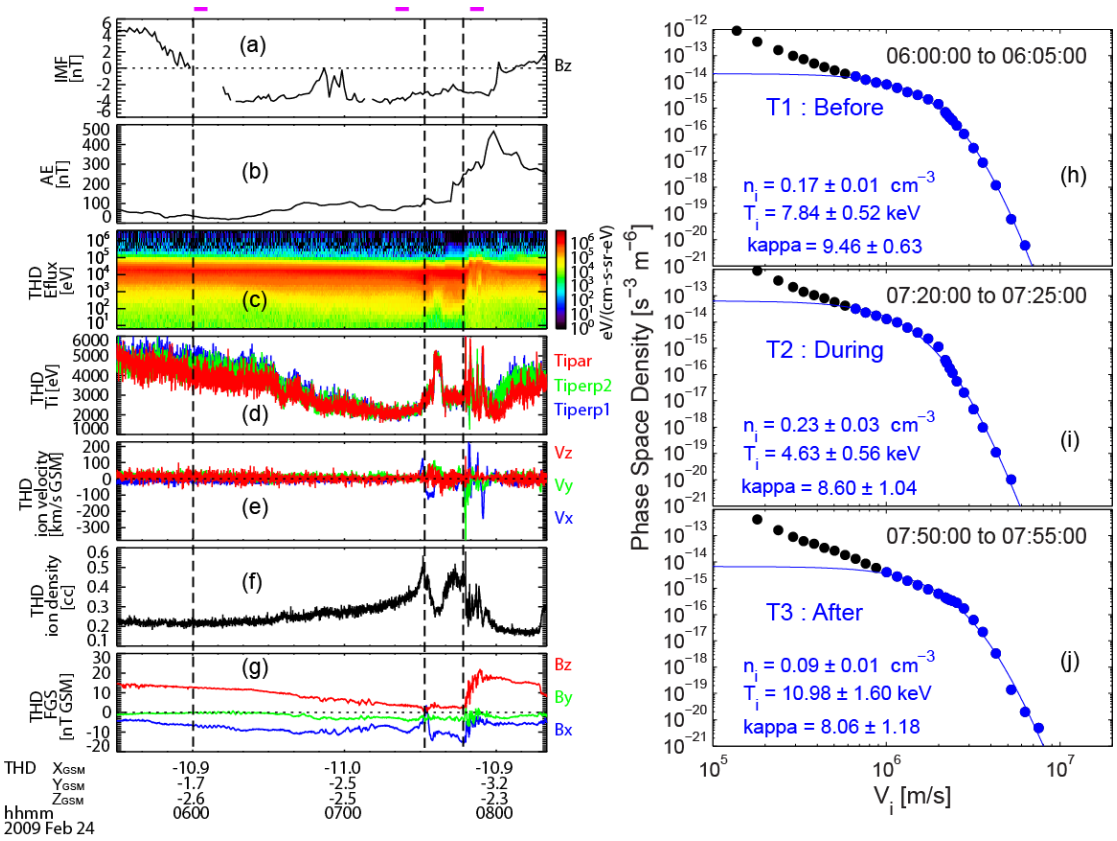

Figure 2. THD observations of a magnetospheric substorm at Earth. (a) IMF B_z from OMNI; (b) auroral ejection index (AE); (c) ion energy spectrum in differential energy flux; (d) ion temperature; (e) ion bulk velocity, (f) ion density; (g) B_x (blue), B_y (green), B_z (red); (h) averaged ion PSD from 06:00 to 06:05 UT, at the beginning of substorm growth phase (T1); (i) averaged ion PSD from 07:20 to 07:25 UT, near the end of substorm growth phase (T2); and (j) averaged ion PSD from 07:50 to 07:55 UT, after the substorm dipolarization (T3). Blue lines in Figures 2h to 2j are the kappa fitting results for the main component PSDs shown in blue. The magenta marks above panel (a) indicate the durations for T1, T2, and T3, respectively.

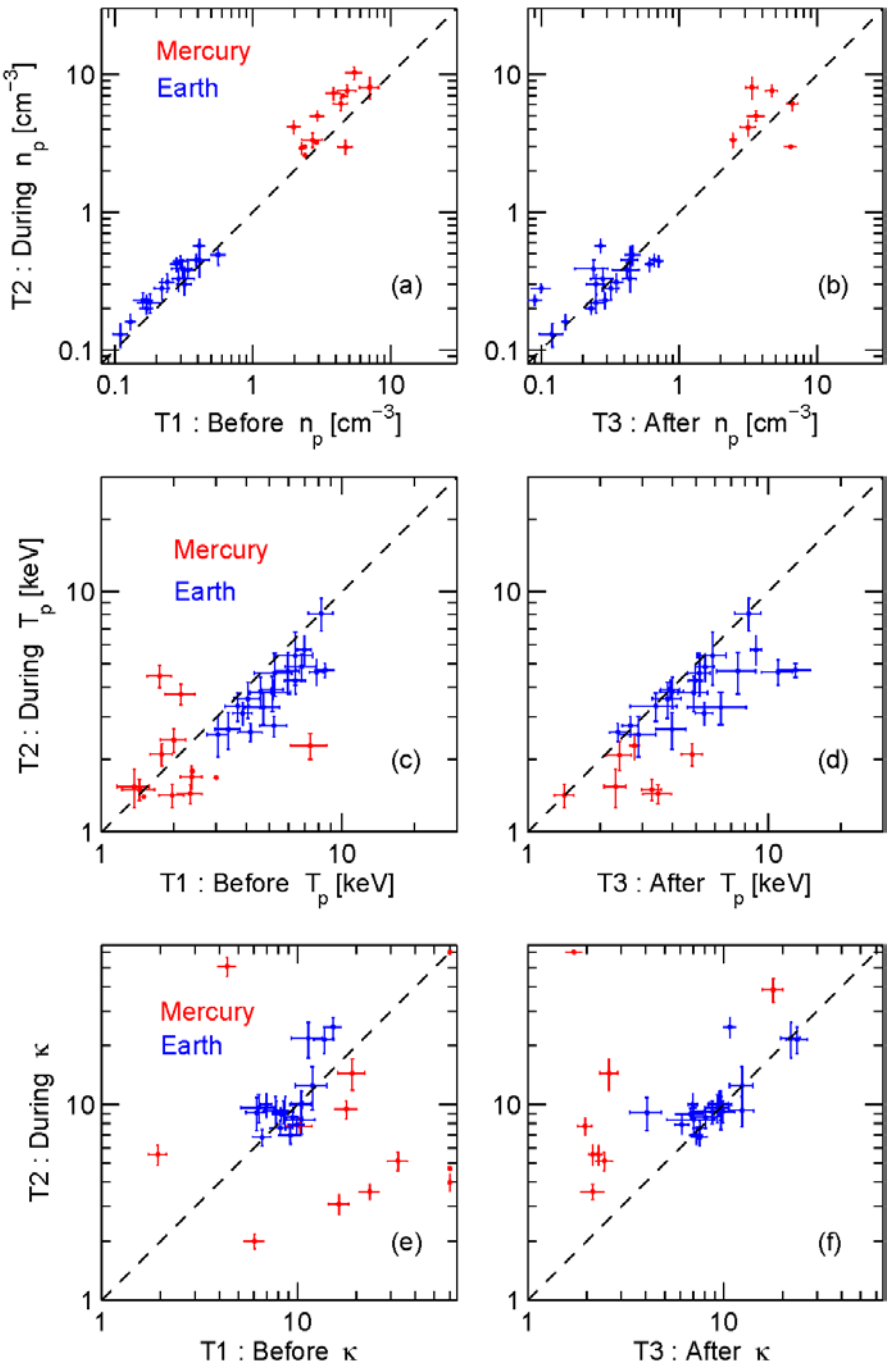

Figure 3. Distributions of proton densities (n_p), temperatures (T_p), and kappa values (κ) during the magnetospheric substorms at both Earth (blue) and Mercury (red). (a) n_p at T1 and T2, (b) n_p at T2 and T3, (c) T_p at T1 and T2, (d) T_p at T2 and T3, (e) κ at T1 and T2, and (f) κ at T2 and T3.

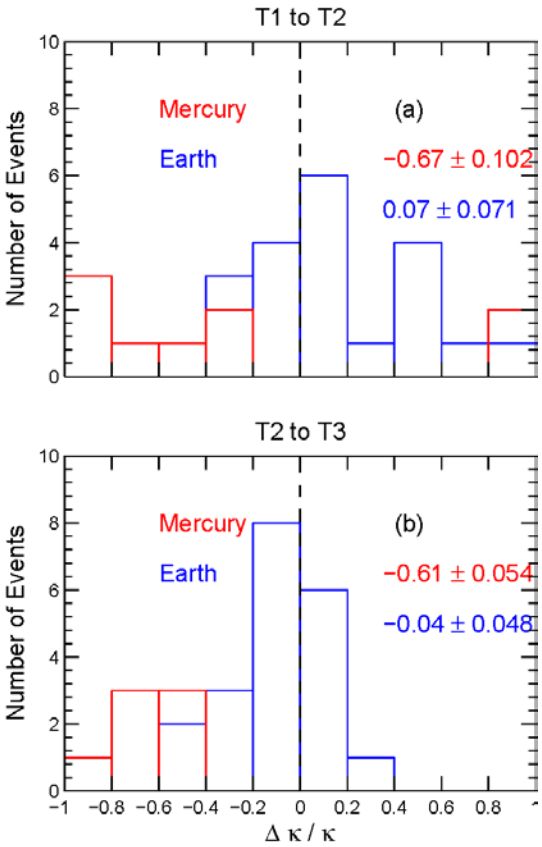

Figure 4. The distributions of the relative κ changes (Δκ/κ). (a) The distribution of Δκ/κ from T1 to T2, and (b) from T2 to T3.

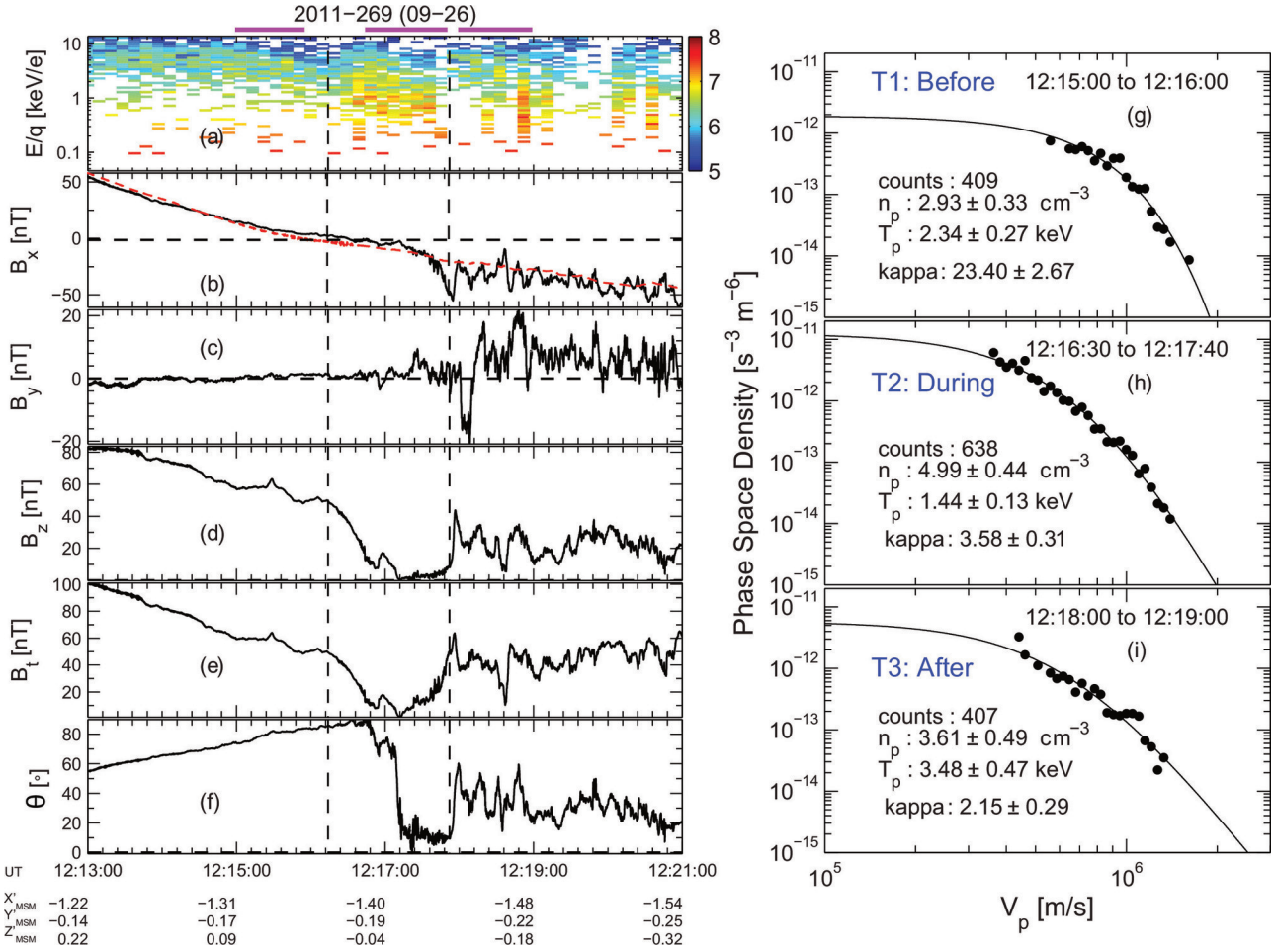

2018gl079181-f01-z-.eps

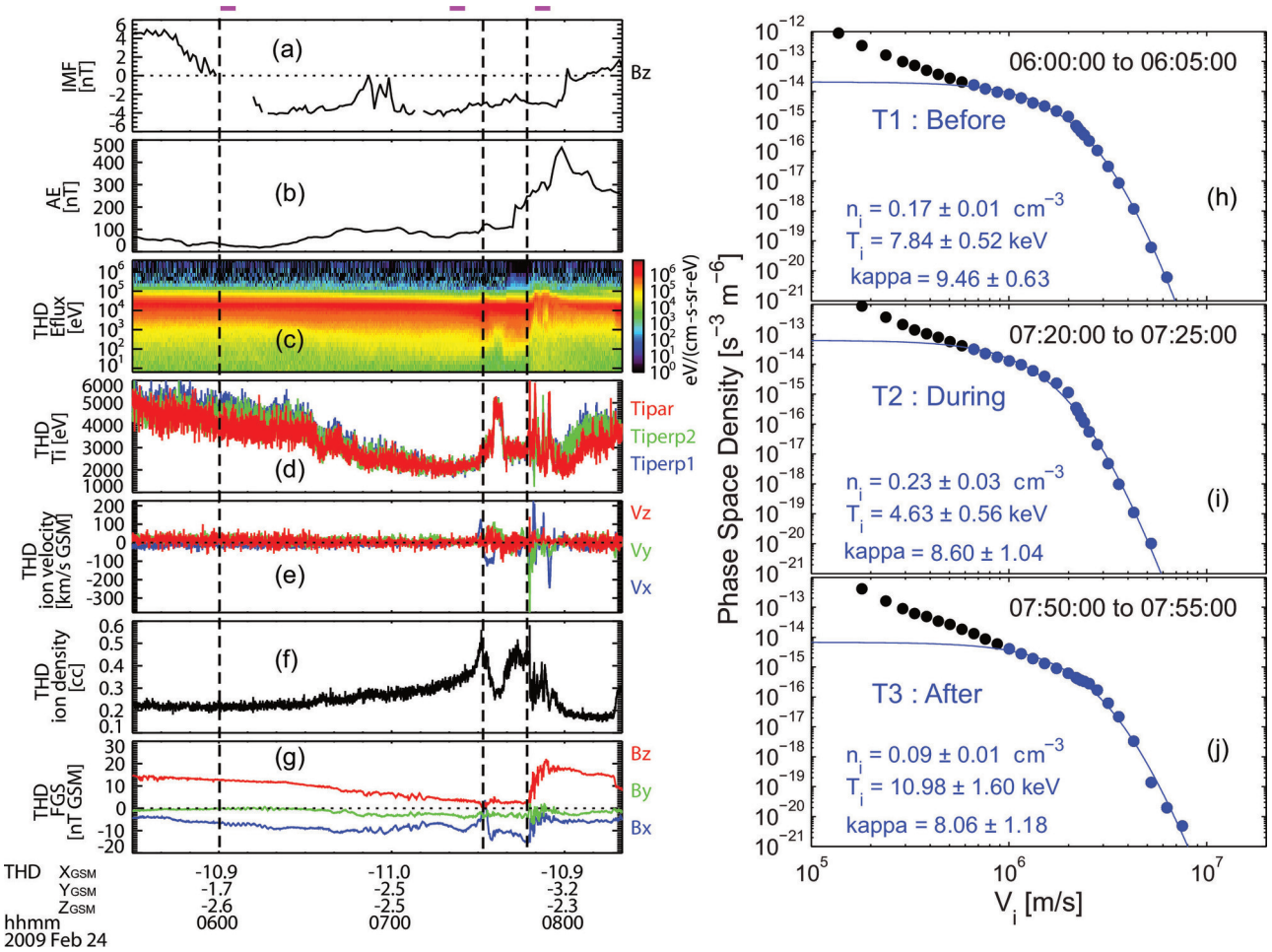

2018gl079181-f02-z-.eps

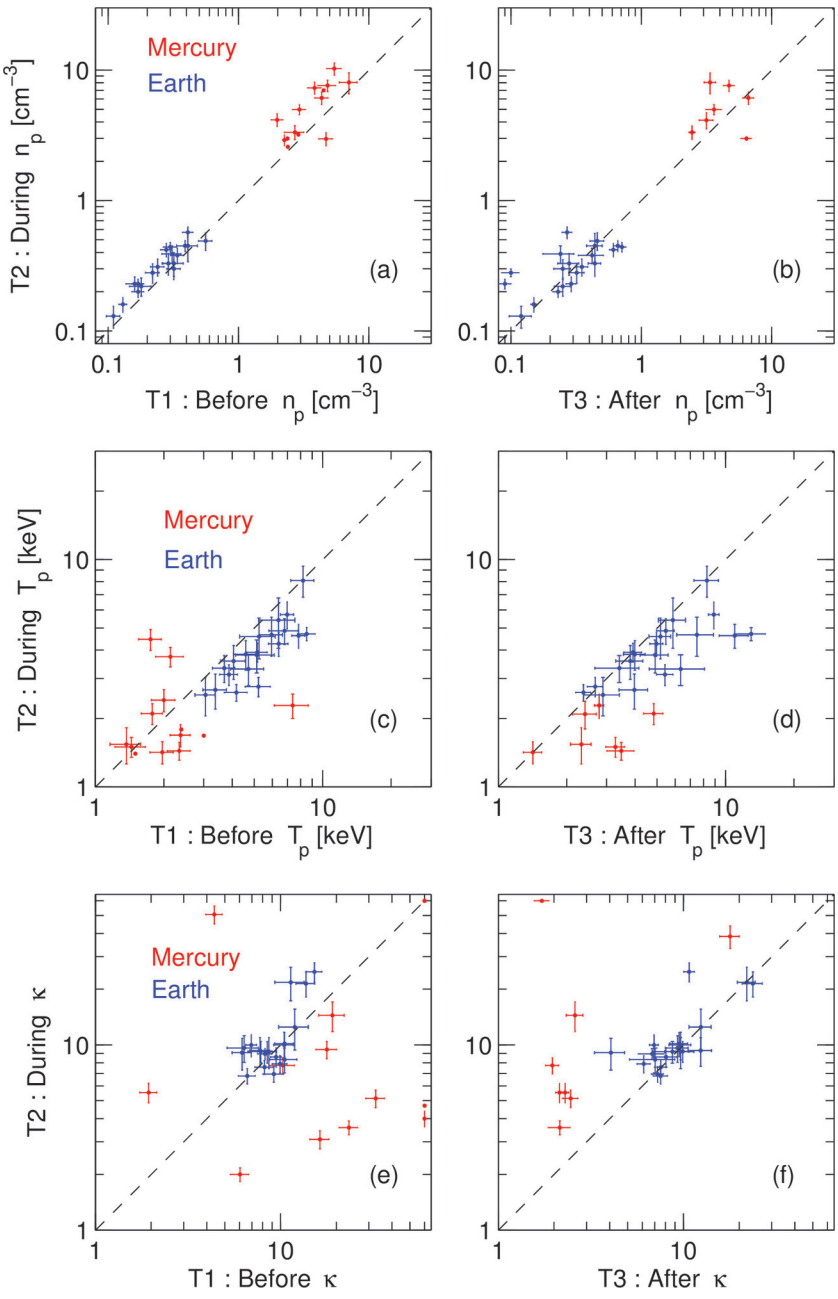

2018gl079181-f03-z-.eps

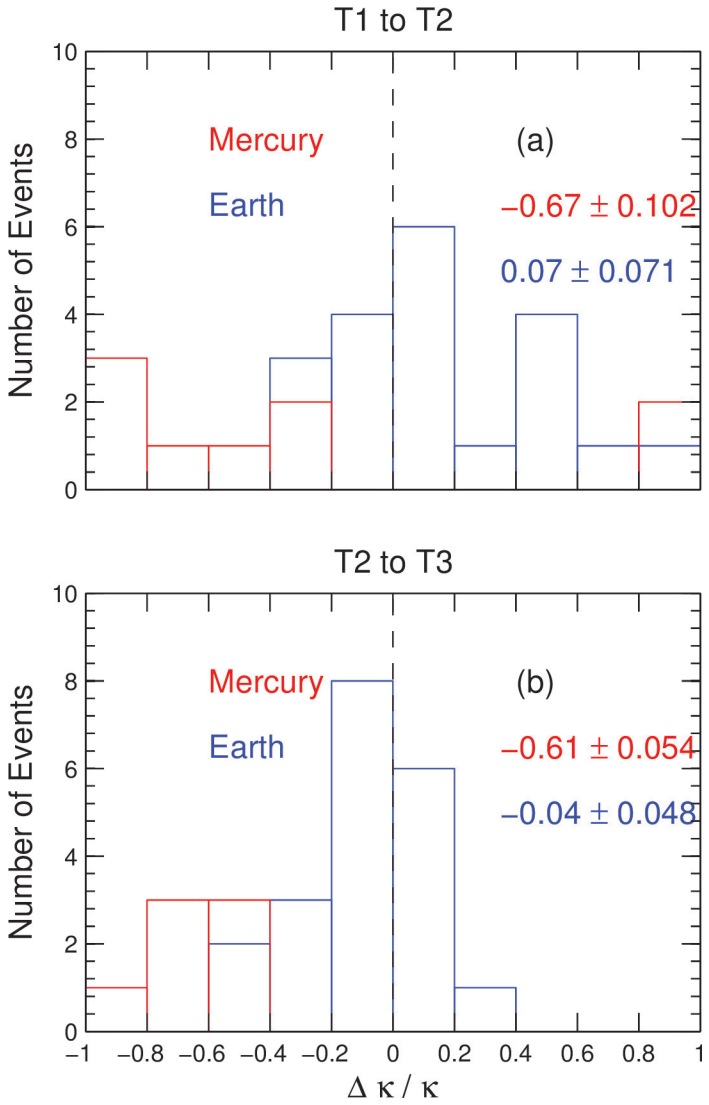

2018gl079181-f04-z-.eps